Journal of Hydrology (2006) **328**, 258–266

available at www.sciencedirect.com

SCIENCE DIRECT®

journal homepage: www.elsevier.com/locate/jhydrol

Use of parameter optimization to estimate a flood wave: Potential applications to remote sensing of rivers

Hélène Roux [a,*], **Denis Dartus** [b]

[a] *Centre d'Etudes Spatiales de la Biosphère (CESBIO), 18 Avenue Edouard Belin, bpi 2801, 31401 Toulouse Cedex 9, France*
[b] *Institut de Mécanique des Fluides de Toulouse, HYDROECO, Allée du Professeur Camille Soula, F-31400 Toulouse, France*

Received 20 July 2005; received in revised form 16 November 2005; accepted 17 December 2005

KEYWORDS
Estimation of river discharge;
Error criterion;
Flood wave;
Inverse problem;
Remotely sensed data

Summary In this paper, the potential for identifying discharge and/or flood hydrograph from remotely sensed data is explored. The parameter identification process is based on the minimization of the difference between the solution of the model equations and the observed system response which consists in maximum inundation extent. The river geometry is supposed to be known, effect of the accuracy of these data on the estimation has been tested. Sensitivity of the model to individual parameters is then assessed using an extension of the generalized sensitivity analysis. Synthetic data have been used to test the methodology. Results show that the Nash criterion of the estimated flood hydrograph is higher than 0.9 for all the tested cases.

Introduction

According to Bjerklie et al. (2003) and Fekete et al. (1999), less than 60% of the runoff from the continents is monitored at the point of inflow in the ocean, and the distribution of runoff within the continent is even less monitored. Moreover, the number of operating hydrometric gauges is decreasing since 1980s, the delivering time is often greater than several months, and there is a great disparity in the gauges spatial distribution (Bjerklie et al., 2005; Seyler, 2003). Barrett (1998) points out that hydrographic data obtained from satellites and other remote sources offer the possibility of broad and potentially frequent global coverage of river discharge estimates. Estimating river discharge using remotely sensed data may then be a mean to increase the global streamflow monitoring network. Moreover, remote sensing is able to provide information over large areas, including those where ground-based data is difficult to obtain. There is therefore a need to develop discharge estimation procedures that do not require ground-based information. Estimating dis-

* Corresponding author.
E-mail address: roux@imft.fr (H. Roux).

0022-1694/$ - see front matter © 2006 Elsevier B.V. All rights reserved.
doi:10.1016/j.jhydrol.2005.12.025

Notation

A	cross-sectional area [m^2]
B	flow top width [m]
B_0	main channel width [m]
g	gravitational acceleration (9.81 m s^{-2})
H	water depth [m]
L_{sill}	sill length [m]
ℓ	parameter affecting the length of the generated flood wave
n	Manning roughness coefficient [s $m^{-1/3}$]
P	sill height [m]
Q	discharge [m^3 s^{-1}]
Q_b	base flow [$m^3.s^{-1}$]
Q_p	peak flow [$m^3.s^{-1}$]
R_H	hydraulic radius [m]
S_f	friction slope (slope of energy grade line) [m m^{-1}]
t	time [s]
t_p	time to peak [s]
U	cross-sectional averaged velocity [m s^{-1}]
x	distance along the channel [m]
$\mathbf{X}$	model state vector
Z	stage [m]
μ_D	energy-loss coefficient of the sill
σ	noise level, standard variation of noise within a sample
Φ	performance function

Superscripts

o	observed value
s	simulated value

Subscripts

L	related to the left bank
R	related to the right bank

charge in river from hydraulic information obtained exclusively from aerial and satellite platforms has been explored by Bjerklie et al. (2003), Bjerklie et al. (2005) and Smith (1997). They mainly develop general relationships between river characteristics than can be observed from space-based platforms and river discharge.

The methodology presented in this paper takes advantage of optimization methods to minimize discrepancies between simulations and observations of flood extent fields in order to estimate river discharge. As assessed before, there is a clear case for the estimation of effective values of discharge from space observations. Water surface width can be measured from a variety of sensors and imagers mounted on satellites and aircrafts. The accuracy of the water surface estimates measured from the images is, in part, a function of the resolution of the images and the accuracy of the measuring tool (Bjerklie et al., 2005). For instance, panchromatic images have spatial resolution as high as a few meters and synthetic aperture radar (SAR) imagers as high as 10 m (Bjerklie et al., 2003). However, width estimates using any imagers may be subject to other errors associated for instance with clouds, vegetation obscuring the banks or wind roughening in the case of SAR. Valley and channel features such as channel length can be observed from different data sources including visible images, DEMs and topographic map information (Bjerklie et al., 2003).

This paper presents an analysis of the possibility to monitor discharge from space using imaging sensors. The analysis is carried out by applying a Saint-Venant based routing routine to a flood wave in a synthetic river channel. The routing parameters are identified by minimizing the difference between simulated and observed river top widths. The channel geometry and flow resistance variables are known. An evaluation of the uncertainties introduced by errors in the observations of the river channel surface is also proposed. The paper initially describes the model which has been applied, and then it discusses the sensitivity analysis. This is followed by a presentation of the parameter identification procedure and the results. Results presented in this paper have been obtained with synthetic data that have been used in order to develop the method. Implementations using field data are now in progress.

Approach

Model description

One-dimensional flow routing approaches still form the majority of traditional numerical models used in practical river engineering (Pappenberger et al., 2005). Moreover, when Horritt and Bates (2002) compared 1D and 2D model codes (HEC-RAS, LISFLOOD-FP and TELEMAC-2D) in an optimization framework, they found that in some cases, 1D models may be very effective in predicting flood extent. Therefore, the model that has been developed solves the one-dimensional Saint-Venant equations:

$$\begin{aligned} &\frac{\partial A}{\partial t}+\frac{\partial Q}{\partial x}=0 \\ &\frac{\partial Q}{\partial t}+\frac{\partial}{\partial x}(QU)+gA\left(\frac{\partial Z}{\partial x}+S_f\right)=0 \end{aligned} \tag{1}$$

where A is the cross-sectional area, Q the discharge, U the cross-sectional averaged velocity, g the gravitational acceleration, Z the stage, S_f the friction slope: $S_f=\frac{n^2Q^2}{R_H^{4/3}A^2}$, n the Manning roughness coefficient, R_H the hydraulic radius, t the time and x the distance along the channel.

The compound channel modeling considered uses the Einstein formula which supposes the equality of friction slopes and velocities in all the cross-sectional subdivisions (Carlier, 1982; USACE, 1997):

$$\begin{cases} S_f|_i = S_f|_{i+1}, & i=1,\ldots,I \\ U|_i = U|_{i+1}, & i=1,\ldots,I \end{cases} \tag{2}$$

$S_f|_i$ is the friction slope of subdivision i, $U|_i$ the averaged velocity of subdivision i and I the total number of subdivisions in the cross-section. It allows calculation of a composite coefficient of roughness, function of the water depth.

Case study

The basis for the gauged data to be used in the identification process was generated by simulating a hydrodynamic wave through a 5 km long model river. Fig. 1 represents the uniform channel cross-section. The channel roughness was chosen to be representative of natural rivers with a Manning value of 0.033 s $m^{-1/3}$ for the main channel and 0.1 s $m^{-1/3}$ for the overbanks. The upstream inflow $Q(x = x_1, t)$ at time t was generated by the following formula (Khatibi et al., 1997):

$$Q(x = x_1, t) = Q_b + Q_p \times \left[\frac{t}{t_p} \exp\left(1 - \frac{t}{t_p}\right)\right]^{\ell} \quad (3)$$

The chosen parametric values are the following: base flow $Q_b = 100\ m^3\ s^{-1}$, peak flow $Q_p = 500\ m^3\ s^{-1}$, time to peak $t_p = 5 \times 10^3$ s and exponent $\ell = 16$. The value of the parameter ℓ affects the length of the flood wave as it can be seen in Fig. 2. A flow depth relationship based on the Manning equation was assumed to describe the downstream boundary condition:

$$H(x = x_J, t) = \left(\frac{Q(x = x_J, t)}{\mu_D L_{sill}\sqrt{2g}}\right)^{2/3} + P \quad (4)$$

where $H(x = x_J, t)$ is total head, $\mu_D = 0.38$ an energy-loss coefficient, $L_{sill} = 50$ m sill length and $P = 4$ m sill height. In order to solve the Saint-Venant unsteady flow equation, the state of flow — $Z(x, t = 0)$ and $Q(x, t = 0)$ — must be known at all cross-sections at the beginning of the simulation. The initial condition has been chosen as steady flow condition: discharge at $t = 0$ is equal to base flow $Q_b = 100\ m^3\ s^{-1}$ at each cross-section. The stage $Z(x, t = 0)$ associated with the steady flow is computed by solving the steady-state Saint-Venant equations using the fourth-order Runge—Kutta method.

These data were sufficient to simulate inflow flood wave through the model river. The system of governing Eq. (1) is approximated using the Preissmann four-point scheme (Pre-

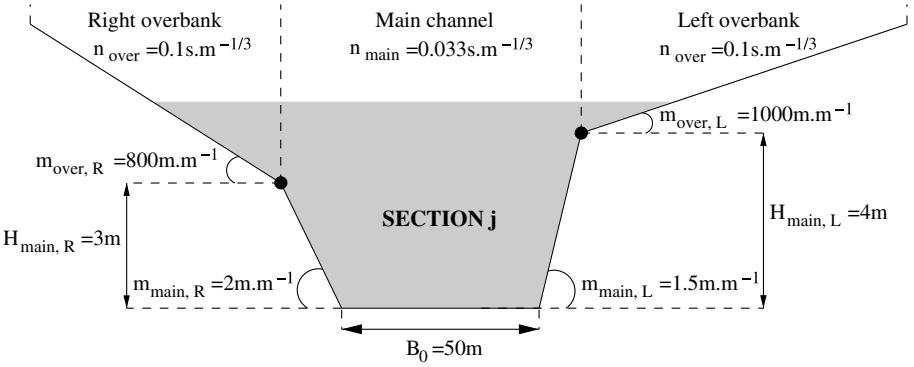

Figure 1 Representation of the uniform channel cross-section.

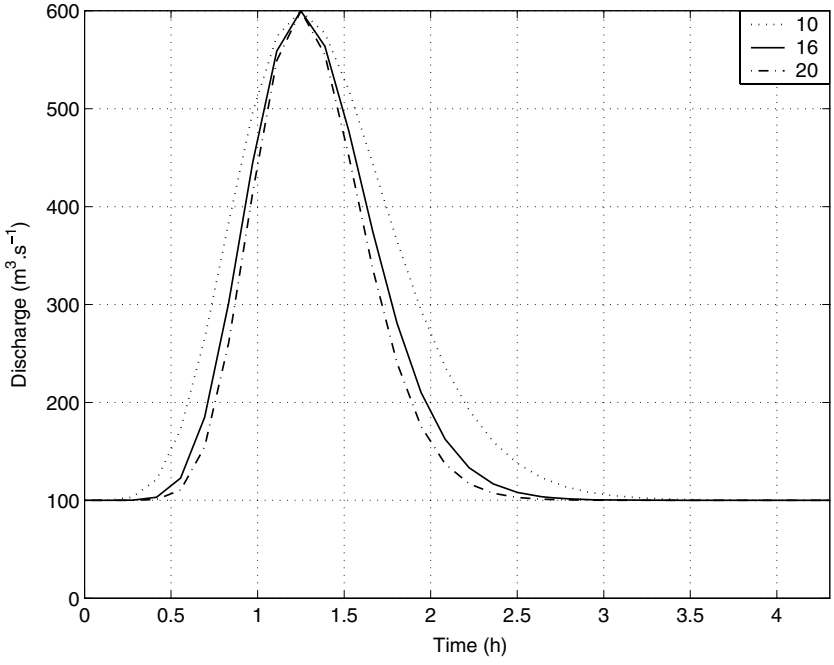

Figure 2 Effect of the value of the length of the flood wave ℓ on the shape of the hydrograph.

issmann, 1961). The resulting system of finite difference is solved by a direct decomposition method called double sweep method or Thomas algorithm (Langendoen, 2000). The channel has been divided into sectional nodes spaced out at 100 m. The simulation was carried out using a time step Δt of 500 s and an implicit difference weighting factor of 2/3. The total duration of the simulation is of 15,500 s.

The numerically true simulated values where obtained by running the model to predict the discharges and stages throughout the system. Knowing the stage and the cross-section geometry, it is then possible to calculate the true extent of the flow $B(x,t)$ throughout the system, which is the basis for the generation of the observation data necessary for identification of the discharge.

Discharge estimating methodology

Identification procedure

Flow state equations describe open-channel hydrodynamics through a number of complex equations in terms of discharge and stage. These equations involve geometric and hydrometric parameters and sometimes a number of empirical parameters specifying the system particulars. Given the values of these parameters, it is possible to solve the Saint-Venant equations to simulate the flow conditions. As some open-channel parameters often lack exact values, flow-state equations may be formulated to ascertain the values of these parameters. The formulation of flow-state equations to this end is referred to under the generic name of inverse problem (Khatibi et al., 2001). This study formulates Saint-Venant based equations to estimate the upstream boundary inflow of a flood event.

The inverse problem is formulated as a non-linear optimization model. $\mathbf{X}$ is the vector of unknown parameters. The unknown parameters will be selected so as to minimize an objective function that measures the distance between the numerical solution and the observations (Eq. (5)). This distance is chosen as the sum of squares of the differences between the simulated and measured values of flow top width: it is a widely used error criterion in hydrology (Nash and Sutcliffe, 1970).

$$\Phi(\mathbf{X}) = \sum_{j=1}^{J} \left((B_j^o - B(\mathbf{X})|_j^s)^2 \right) \quad (5)$$

j is the spatial subscript. It varies recursively from 1 to J, J being the number of cross-sections. B_j^o is the observed flow top width of cross-section j and $B(\mathbf{X})|_j^s$ is the flow top width at cross-section j, simulated using the estimated parameters $\mathbf{X}$. In order to minimize the performance function Φ in Eq. (5), an iterative minimization procedure is required (Ding et al., 2004). The minimization is carried out using traditional algorithms based on the non-linear least square technique (Madsen, 2003): a quasi-Newton method has been chosen in this study.

The numerical test procedure consists of two steps: (i) selecting a set of reference parameters $\mathbf{X}_{ref}$, solving the flow equations to generate the basis for the observed data. The numerically true simulated values at each computational node are then contaminated with Gaussian noise in order to emulate remote sensing data, $\mathbf{B}^o$ (Following §). (ii) The inverse problem is implemented to identify the set of reference parameters $\mathbf{X}_{ref}$ from the observations $\mathbf{B}^o$ (i.e. the flow top widths contaminated with noise).

Generation of gauged data

Assuming that noise contained in satellite data is normally distributed, noise-free top width values $\mathbf{B} = B(x,t)$, as described above, were contaminated with Gaussian noise, emulating satellite data. Samples of data-errors have been generated by changing the seeding of the random number generator with a prescribed noise level σ, allowing a study of the effect of data-errors on the identified parameters, similar to Khatibi et al. (2001). Noise level σ refers to the standard deviation of noises within a sample. Six noise levels have been introduced, resulting in an average variation of flow top width at nodal points $|\overline{\mathbf{B}^o - \mathbf{B}}|$ from 1 to 4 m (Table 1) which is approximately the resolution that can be provided by the panchromatic images of IKONOS for instance. At the maximum extent, averaged flow top width is about 3 km.

The use of synthetic data provides the following facilities: (i) as the true value of the parameters to be estimated is known, it becomes possible to evaluate the performances of the proposed model; (ii) there is no restriction on the number of synthetically-generated gauged events whereas the field data are often scarce. Notwithstanding the above, synthetic data cannot replace field data, as a model theoretically studied using synthetic data has to be tested using field data. As already discussed in the introduction, both water surface width and water surface area can be measured from satellites or aircrafts. Panchromatic imagers have spatial resolution as high as 1 m (1 m for IKONOS, 2.5 m for SPOT 5) and SAR imagers as high as 5 m (5 m for NASA/JPL AIRSAR, 10 m for ERS-1 SAR). However, the ability of a sensor to observe water surface width not only depends on the imager resolution. Indeed, width estimates are subject to errors associated with vegetation obscuring the water surface and clouds, or surface wind in the case of SAR which can observe through the cloud cover. To improve the accuracy, the width can be estimated by dividing the measured total water surface area of the reach by the reach length. In that case, a suggested reach length for averaging is at least 10 times the channel width. Bjerklie et al. (2005) uses aerial photos at 1:10,000 scale and found an accuracy for width measurement of approximately 4 m. They also emphasize the fact that the accuracy would generally be greater for large rivers.

Table 1 Induced data error for each noise level, $|\overline{\mathbf{B}^o - \mathbf{B}}|_{L\,or\,R}$ is the variation of flow top width for each bank, $|\overline{\mathbf{B}^o - \mathbf{B}}|$ is the total variation of flow top width

Noise level σ	$\lvert\overline{\mathbf{B}^o - \mathbf{B}}\rvert_{L\,or\,R}$ (m)	$\lvert\overline{\mathbf{B}^o - \mathbf{B}}\rvert$ (m)
No. 1 (lowest)	0.5	0.7
No. 2	1.0	1.4
No. 3	1.4	2.0
No. 4	1.9	2.7
No. 5	2.4	3.4
No. 6 (highest)	2.9	4.0

Another constraint of remote sources is the repeat cycle: high resolution data have to be consistently acquired at a high frequency to detect brief flood event (Smith et al., 1996). In that case, aerial observations can provide denser time series than satellite ones.

Sensitivity to individual parameters

In this section, part of the generalized likelihood uncertainty estimation (GLUE) methodology is introduced; it will then be implemented to assess sensitivity of the model to individual parameters. A widely used criterion, the efficiency of the model (Eq. (6)), is taken as a measure to evaluate model predictions.

Methodology of the sensitivity analysis

GLUE is a Bayesian Monte-Carlo method which allows that different parameter sets within a model structure might perform equally well in reproducing the observations (Beven and Binley, 1992; Freer et al., 1996; Pappenberger et al., 2005). Uncertainty is generic to the application of environmental models and it might be difficult to decide between different sets of effective parameter values (Beven, 2004). The result is the equifinality problem, defines by Beven (1993). In GLUE, this problem is acknowledged by running the model with different randomly chosen sets of parameter values. The procedure used in this study can be summarized as follows (Beven and Binley, 1992; Freer et al., 1996):

Step 1. Definition of a likelihood measure intended as a measure of how well the model conforms to the observed behavior of the system. An example of likelihood measure is the model efficiency $\mathscr{L}_e$, defined by

$$\mathscr{L}_e = 1 - \frac{\sigma_e^2}{\sigma_o^2},\ \sigma_e^2 < \sigma_o^2 \tag{6}$$

where σ_e^2 is the variance of the errors and σ_o^2 is the variance of the observations, that is to say, for this study:

$$\mathscr{L}_e = 1 - \frac{\sum_{j=1}^{J}((B_j^o - B(\mathbf{X})|_j^s)^2)}{\sum_{j=1}^{J}((B_j^o - \overline{B^o})^2)} \tag{7}$$

$\overline{B^o}$ is the average of the observed flow top widths.

Step 2. Definition of the initial range or distribution of parameter values to be considered. Uniform distributions are mainly used in lack of prior information.

Step 3. Monte-Carlo simulations achieved by running the model with different randomly chosen sets of parameter values. Each set of parameter values is assigned a likelihood of being a simulator of the system, on the basis of the chosen likelihood measure.

Step 4. Sensitivity to individual parameters. The sensitivity of the model predictions to the individual parameters can be tested by using the generalized sensitivity analysis (Hornberger and Spear, 1981). The authors constructed distributions for each parameter conditioned on a classification of the Monte-Carlo simulations into two classes: behavioral and non-behavioral. The criterion for differentiating between the two classes is a subjectively chosen value of a goodness of fit measure, like the likelihood measure used in the GLUE procedure. A strong difference between distributions reveals a sensitive parameter. A direct measure of the separation of the cumulative distribution functions can be the statistic d_{rs} used in the Kolmogorov–Smirnov two sample test:

$$d_{rs} = \sup_X |S_r(X) - S_s(X)| \tag{8}$$

where S_r and S_s are the sample distribution functions of the parameter X corresponding to the cumulative distribution functions of the behavioral and non-behavioral categories respectively, for r behaviors and s non-behaviors. Large values of d_{rs} indicate that the parameter is important for simulating the behavior. However, this is only a univariate analysis, it is possible that cumulative distribution functions of one parameter exhibit no separation under the behavioral classification and yet this parameter could be crucial to a successful simulation, by virtue of a strong correlation with other parameters under the behavior.

Results

Sensitivity to 4 parameters has been tested. Ranges of variation of the parameters are listed in Table 2. Prior parameter distributions have been chosen uniform. The behavior criterion is defined as followed: (i) $\mathscr{L}_e > 0.8$: simulations behavioral, (ii) $\mathscr{L}_e \leqslant 0.8$: simulations non-behavioral.

Of 5000 simulation runs conducted in the Monte-Carlo experiments, 1132 fell in the behavior category with 3868 in the non-behavior class. In Fig. 3 it can be seen that good and poor simulations are available throughout the same parameter range. It suggests that the parameter response surface is very complex and confirms that the value of a single parameter has little meaning when taken outside the context of the values of the other parameters.

A ranking of individual parameters on the basis of the separation in the distribution functions (Eq. (8)) classified 1 of the 4 parameters as unimportant for mimicking the behavior (Table 3). Values of the flow top width seems to be very sensitive to the base flow Q_b. Parameters Q_p, t_p and ℓ show a large range of equifinality. Next step will be to test the possibility of identifying the hydrograph using a traditional optimization method.

Estimating river discharge

Implementation of the optimization method

In a first step, the discharge along the channel at the initial time $Q(x, t = 0)$ is estimated. Then, starting from this initial condition, the identified discharge along the channel, the discharge at the upstream boundary for each time step

Table 2 Parameter ranges used in Monte-Carlo simulations

Parameter	Description	Minimum	Maximum
Q_b	Base flow ($m^3\ s^{-1}$)	90	110
Q_p	Peak flow ($m^3\ s^{-1}$)	450	550
t_p	Time to peak (s)	4500	5500
ℓ	Length of flood wave (−)	14.4	17.6

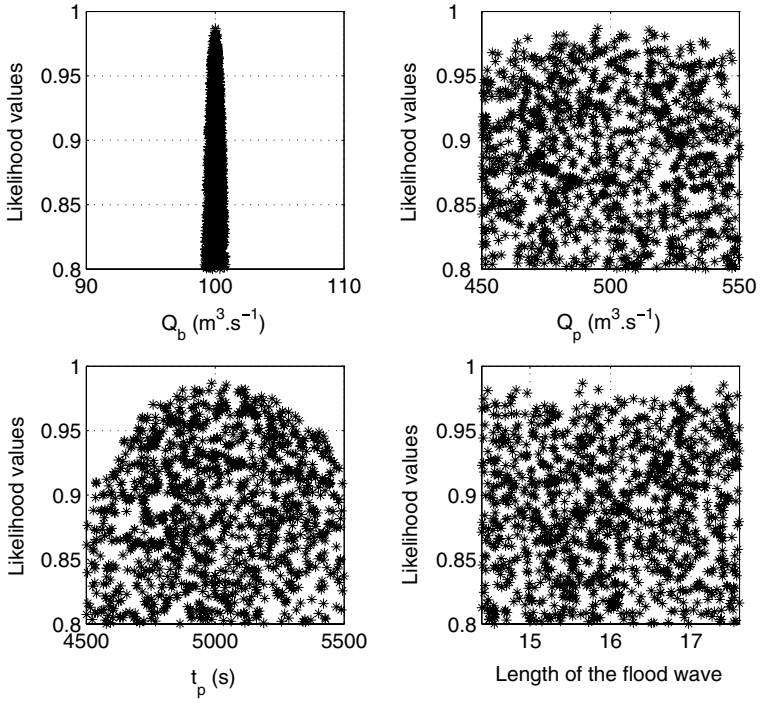

Figure 3 Scatter plot of efficiency results for each parameter in Monte-Carlo simulations; likelihood measure of Eq. (7).

Table 3 Ranking of individual parameters on the basis of the Kolmogorov–Smirnov statistic and corresponding level of significance for 1132 behavioral simulations of 5000 simulation runs

Parameter	d_{rs}	Level of significance (%)
Q_b	0.29	>99.9
t_p	0.10	>99.9
Q_p	0.06	>99.5
ℓ	0.03	<90.0

$Q(x = x_1, t)$ is estimated. The cross-section geometry is considered as known (Fig. 4(a)). The true values of the geometric parameters — depth, slope, flow resistances — have been contaminated with Gaussian noise for the emulation of noise normally contained in field data (Fig. 4(b)). These geometric data are necessary to estimate discharge according to the methodology that has been implemented here. Channel features such as channel slope can be observed from DEMs and topographic map information, the channel width can be measured from different sensors and imagers in the same way as the water surface width (§ Generation of gauged data). Lots of work has been done in the estimation of riverbed roughness, see for instance Khatibi et al. (1997); Atanov et al. (1999); Werner et al. (2005), but there are only few attempts to retrieve information on riverbed geometry using remote sensing observations (Roux and Dartus, 2005). Measuring or estimating these variables from remote sources still remains a difficult task.

Performance function

In order to take into account the asymmetry of the flooded area, the chosen objective function represents the sum of squares of the differences between gauged flow top widths and simulated flow top widths for each bank. At each time step, the objective function is formulated as follows:

$$\Phi(\mathbf{X}^k) = \sum_{j=1}^{J} \left(\left(B^o|_j^k - B^s(\mathbf{X}^k)|_j^k \right)_R^2 + \left(B^o|_j^k - B^s(\mathbf{X}^k)|_j^k \right)_L^2 \right) \quad (9)$$

k is the temporal superscript. The subscript R concerns the values related to the right bank, the subscript L the ones related to the left bank.

This performance function is minimized at each time step. At $t = 0$, $\mathbf{X}^0$ is the discharge along the channel: $\mathbf{X}^0 = Q(x, t = 0)$; for $t = k$, k varying from 1 to K, $\mathbf{X}^k$ is the discharge at the upstream boundary: $X^k = Q(x = x_1, t = k)$.

The following results have been obtained by assimilation of 32 data sets, each set is a (51,1) vector of noisy flow top widths at time $t = k$. For each time step and for each noise level σ, 30 gauged samples have been generated by changing the seeding of the random number generator as explained before. Sample here is used in the sense of gauged event. All the figures in this section represent an average of the identified values of each 30 samples of the different data sets. The initial estimates of the parameters and the bound constraints of the algorithm are listed Table 4.

Identification of the initial state of flow

If the geometry is known exactly (Fig. 4(a)), that is to say without introduction of noise, estimates of the initial discharge at nodal points oscillate around the true value as it can be seen on Fig. 5. Further investigation was also carried out using Student's t distribution to calculate confidence intervals (Khatibi et al., 2001). If we consider the mean of the estimates at nodal points, the identified value varies

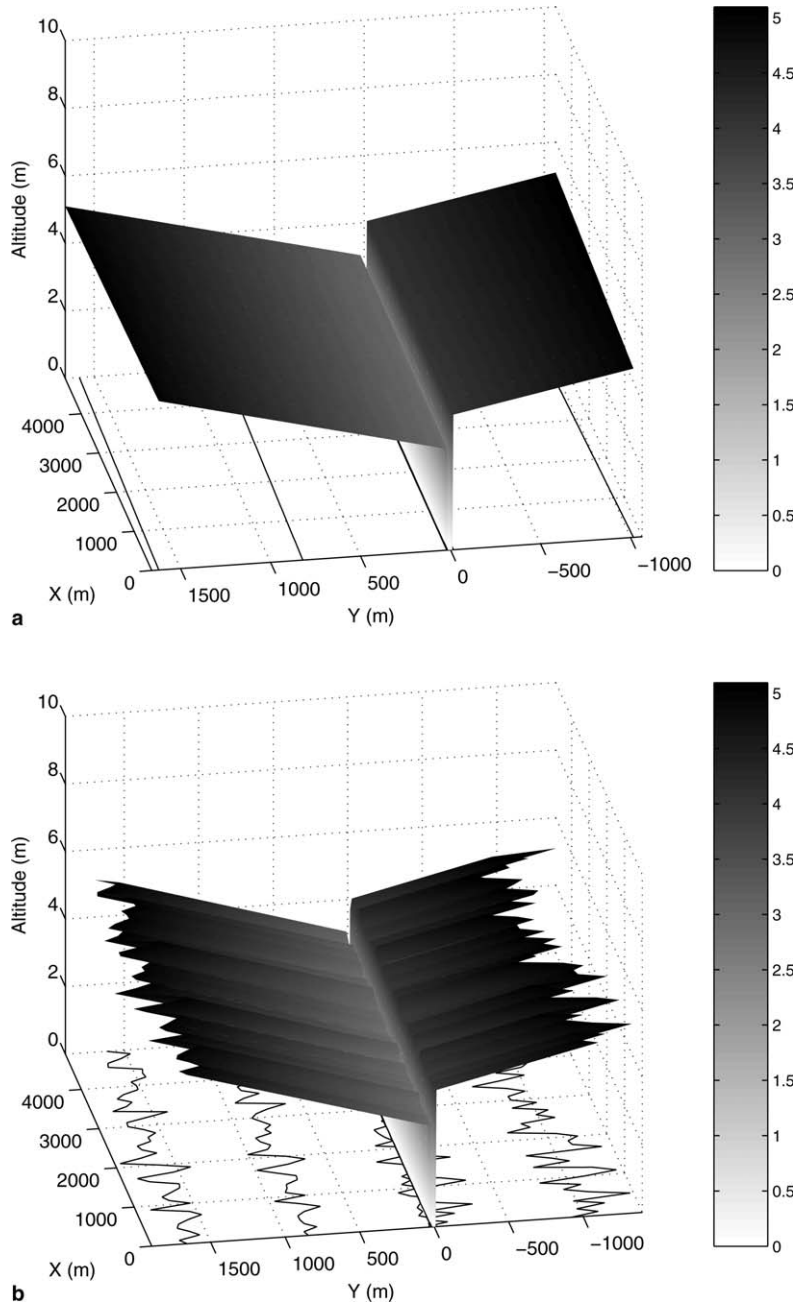

Figure 4 (a) Noise free geometry, (b) geometry contaminated with Gaussian noise.

Table 4 Initial estimates and bound constraints of the minimization algorithm

	$Q(x, t = 0)$	$Q(x = x_1, t = k)$
Initial estimate ($m^3 s^{-1}$)	150	$Q(x = x_1, t = k - 1)$
Lower bound ($m^3 s^{-1}$)	80	100
Upper bound ($m^3 s^{-1}$)	180	1000

from 99.8 $m^3 s^{-1}$ for the lowest observation noise level to 97.9 $m^3 s^{-1}$ for the highest observation noise level. The true value of the initial discharge is estimated with a relative error of less than 2% for each noise level.

When the geometry is contaminated with Gaussian noise for the emulation of measurement uncertainties (Fig. 4(b)), the estimate of the initial discharge could be not satisfactory: it can present a relative error of approximately 30% for each noise level. The oscillations of the estimated discharge may be due to the lack of a prior or background estimate of the parameters. Indeed, for data assimilation methods, regularization may be provided in this form. A new objective function may then be formulated as the sum of a background term and an observation term. The background term measures the distance between the prior and the current estimate; the observation term represents the distance between observation and simulation.

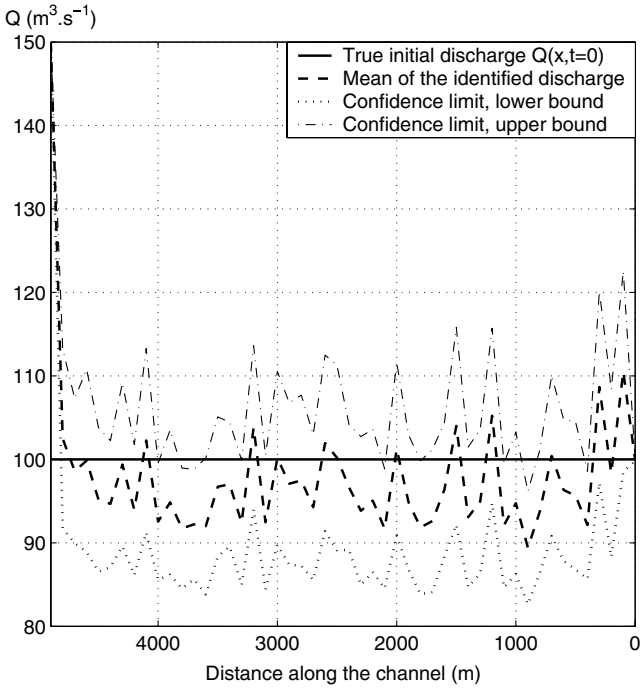

Figure 5 Mean identified initial discharge and confidence interval for the highest observation noise level, noise free geometry.

Identification of the flow at the upstream end

The initial stages at nodal points are calculated by solving the steady-state Saint-Venant equations using the estimates of the initial discharge at nodal points (§ Identification of the initial state of flow). These stages and discharges at nodal points are the initial conditions necessary to solve the Saint-Venant unsteady flow equations. The discharge at the upstream boundary is estimated at each time step by minimization of the performance function (Eq. (9)).

When the geometry is known exactly the upstream discharge is estimated with a Nash criterion (Eq. (10)) of more than 0.99 for all the data noise levels.

$$\text{Nash} = 1 - \frac{\sum_{k=1}^{K}\left(Q_{x=x_1}|^k - Q^s_{x=x_1}|^k\right)^2}{\sum_{k=1}^{K}\left(Q_{x=x_1}|^k - \overline{Q_{x=x_1}}\right)^2} \quad (10)$$

$Q_{x=x_1}|^k = Q(x = x_1, t = k)$ is the true upstream discharge at time $t = k$, $Q^s_{x=x_1}|^k$ is the estimated upstream discharge at time $t = k$ and $\overline{Q_{x=x_1}}$ is the average of the true upstream discharges during the considered period (Nash and Sutcliffe, 1970). Even using the geometry contaminated with Gaussian noise, the discharge at the upstream end of the reach is always identified with a Nash criterion greater than 0.9 (Fig. 6) which is a good performance for flood prevention.

Conclusions

There are lots of applications for remote discharge estimates, for rivers that have poor accessibility, for a global coverage which will provide frequent estimate of discharge over large areas.

The approach presented in this paper uses the most common hydraulic property studied by remote sensing: the inundation extent field (Bates et al., 1997). Measurements of width using remote sources can reach accuracy as high as some meters, as the synthetic gauged data used in this study. The accuracy would generally be greater in the case of large rivers. Moreover, the frequency of satellite observations is not compatible with the tracking of a brief flood

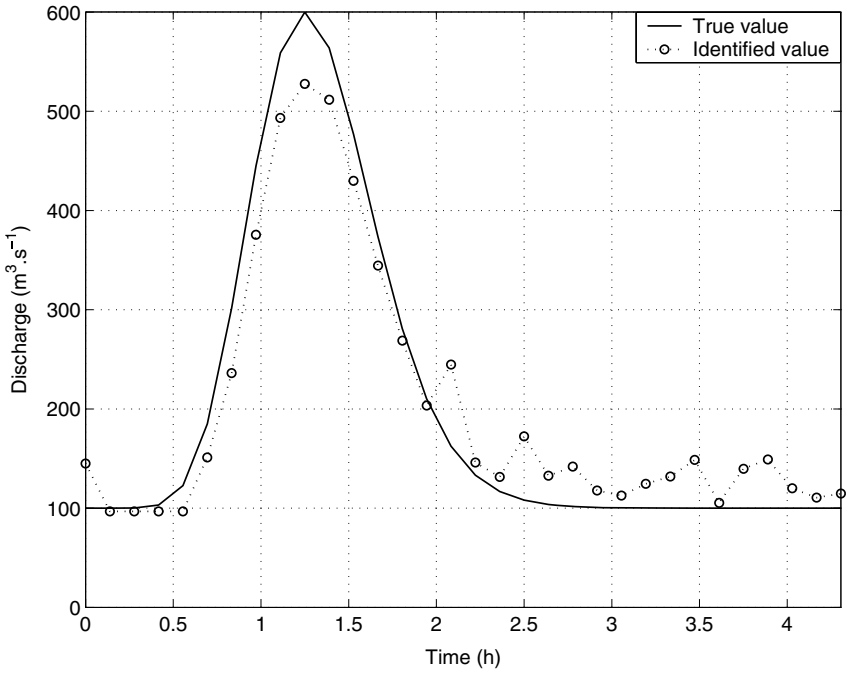

Figure 6 Mean of identified discharge at the upstream end of the reach for the highest observation noise level, geometry contaminated with Gaussian noise.

wave. From these perspectives, potential application of the method presented in this paper to remote sensing can be considered in the context of large rivers. Aerial observations constitute an alternative to obtain denser time series and detect a brief flood wave. The successful use of this methodology will also depend on the ability to measure and/or to estimate river geometry from space. To this end, development and verification of this technology will greatly enhance the potential ability to measure river discharge from space (Bjerklie et al., 2003).

Estimation of discharge over a reach by minimization of an objective function (Eq. (9)) can be used to derive a reach averaged value with reasonable accuracy, provided that the geometry of the river is well known. Estimation of discharge over a time period by minimization of the same objective function (Eq. (9)) gives good results, even when the geometry of the river is contaminated with noise. For all the observation noise levels, a comparison of the estimations with the ''true'' hydrograph shows that the procedure gives good estimates, with accuracy better than 20%. Traditional ground based, non-contact measurements, like the slope-area method usually provide an accuracy of ±20% (Bjerklie et al., 2005), accuracy of the estimate provided using remote sensed information may then be comparable.

A strong point of the methodology of this study is that it is easily adaptable to the new sorts of data that the progresses in telemetry are going to make available in a few years (Smith, 1997). Indeed, satellite altimetry (TOPEX/POSEIDON launched in August 1992, or ENVISAT launched in March 2002) has been able to measure time series of water levels on very large rivers, such as the Amazon (Birkett, 1998; Koblinsky et al., 1993), the Paraná or the Gange. If water levels were also available, the assimilation problem could be formulated in a multi-objective context in which different cost functions those measure different distances, one related to the water level and one related to the flow top width for instance, can be optimized simultaneously. In this framework, the calibration will be tailored to the specific model application being considered (Madsen, 2003).

References

Atanov, G.A., Evseeva, E.G., Meselhe, E.A., 1999. Estimation of roughness profile in trapezoidal open channel. J. Hydr. Eng. ASCE 125 (3), 309–312.

Barrett, E., 1998. Satellite remote sensing in hydrometry. In: Ed, H. (Ed.), Hydrometry: Principles and Practices. Wiley, Chichester, UK, pp. 199–224.

Bates, P.D., Horritt, M.S., Smith, C.N., Mason, D., 1997. Integrating remote sensing observations of flood hydrology and hydraulic modelling. Hydrol. Process. 11, 1777–1795.

Beven, K., 1993. Prophecy, reality and uncertainty in distributed hydrological modelling. Adv. Water Res. 16, 41–51.

Beven, K., 2004. Towards environmental models of everywhere: advances in modelling and data assimilation. In: British Hydrological Society International Conference 2004, Hydrology: Science and Practice for the 21st Century. British Hydrological Society, Imperial College London, UK, pp. 244–250.

Beven, K., Binley, A., 1992. The future of distributed models: model calibration and uncertainty prediction. Hydrol. Process. 6, 179–198.

Birkett, C.M., 1998. Contribution of the TOPEX NASA radar altimeter to the global monitoring of large rivers and wetlands. Water Resour. Res. 34 (5), 1223–1239.

Bjerklie, D.M., Dingman, S.L., Vorosmarty, C.J., Bolster, C.H., Congalton, R.G., 2003. Evaluating the potential for measuring river discharge from space. J. Hydrol. 278, 17–38.

Bjerklie, D.M., Moller, D., Smith, L.C., Dingman, S.L., 2005. Estimating discharge in rivers using remotely sensed hydraulic information. J. Hydrol. 309, 191–209.

Carlier, M., 1982. Hydraulique générale et appliquée. Eyrolles, Paris, France.

Ding, Y., Jia, Y., Wang, S.S.Y., 2004. Identification of Manning's roughness coefficients in shallow water flows. J. Hydr. Eng. ASCE 130 (6), 501–510.

Fekete, B.M., Vorosmarty, C.J., Grabs, W., 1999. Global composite runoff fields based on observed river discharge and simulated water balance. 22, WMO-Global Runoff Data Center, Koblenz, Germany.

Freer, J., Beven, K.J., Amboise, B., 1996. Bayesian estimation of uncertainty in runoff prediction and the value of data: an application of the GLUE approach. Water Resour. Res. 32 (7), 2161–2173.

Hornberger, G.M., Spear, R.C., 1981. An approach to the preliminary analysis of environmental systems. J. Environ. Manage. 12, 7–18.

Horritt, M.S., Bates, P.D., 2002. Evaluation of 1D and 2D numerical models for predicting river flood inundation. J. Hydrol. 268, 87–99.

Khatibi, R.H., Williams, J.J.R., Wormleaton, P.R., 1997. Identification problem of open-channel friction parameters. J. Hydr. Div. ASCE, 123.

Khatibi, R.H., Wormleaton, P.R., Williams, J.J.R., 2001. Parameter quality conditions in open-channel inverse problems. J. Hydr. Res. 38 (6), 447–458.

Koblinsky, C.J., Clarke, R.T., Brenne, A.C., Frey, H., 1993. Measurement of river level variations with satellite altimetry. Water Resour. Res. 29 (6), 1839–1848.

Langendoen, E.J., 2000. CONCEPTS — Conservational Channel Evolution and Pollutant Transport System. 16, United States Department of Agriculture—Agricultural Research Service, National Sedimentation Laboratory, Oxford, USA.

Madsen, H., 2003. Parameter estimation in distributed hydrological catchment modelling using automatic calibration with multiple objectives. Adv. Water Resour. 26, 205–216.

Nash, J.E., Sutcliffe, J.V., 1970. River flow forecasting through conceptual models. Part I — A discussion of principles. J. Hydrol. 10, 282–290.

Pappenberger, F., Beven, K., Horritt, M., Blazkova, S., 2005. Uncertainty in the calibration of effective roughness parameters in HEC-RAS using inundation and downstream level observations. J. Hydrol. 302, 46–69.

Preissmann, A., 1961. Propagation des intumescences dans les canaux et rivières. In: First Congress of the French Association for Computation, Grenoble, France, pp. 433–442.

Roux, H., Dartus, D., 2005. Parameter identification using optimization techniques in open-channel inverse problems. J. Hyd. Res. 43 (3), 311–320.

Seyler, F., 2003. The CASH Project, Workshop on hydrology from space. CNES, Toulouse, France. Available from: <http://gos.legos.free.fr/Presentations_PDF/Seyler.pdf>.

Smith, L.C., 1997. Satellite remote sensing of river inundation area, stage, and discharge: a review. Hydrol. Process. 11, 1427–1439.

Smith, L.C., Isacks, B.L., Bloom, A.L., Murray, B., 1996. Estimation of discharge from three braided rivers using synthetic aperture radar satellite imagery: potential application to ungaged basins. Water Resour. Res. 32 (7), 2021–2034.

USACE, 1997. HEC-RAS River Analysis System, US Army Corps of Engineers, Hydrologic Engineering Center.

Werner, M.G.F., Hunter, N.M., Bates, P.D., 2005. Identifiability of distributed floodplain roughness values in flood extent estimation. J. Hydrol. 314 (1–4), 139–157.